IN-64

191168

39P

NASA Technical Memorandum 106314
ICOMP-93-29

On The Stability Analysis of Approximate Factorization Methods for 3D Euler and Navier-Stokes Equations

A.O. Demuren
Institute for Computational Mechanics in Propulsion
Lewis Research Center
Cleveland, Ohio

and *Old Dominion University*
Norfolk, Virginia

and

S.O. Ibraheem
Old Dominion University
Norfolk, Virginia

October 1993

INSTITUTE FOR COMPUTATIONAL MECHANICS IN PROPULSION
NASA
ICOMP
Lewis Research Center
Ohio Aerospace Institute

NASA

ON THE STABILITY ANALYSIS OF APPROXIMATE FACTORIZATION METHODS FOR 3D EULER AND NAVIER-STOKES EQUATIONS

A.O. Demuren
Institute for Computational Mechanics in Propulsion
Lewis Research Center
Cleveland, Ohio 44135

and Old Dominion University
Department of Mechanical Engineering and Mechanics
Norfork, Virginia 23529

and

S.O. Ibraheem
Old Dominion University
Department of Mechanical Engineering and Mechanics
Norfork, Virginia 23529

SUMMARY

The convergence characteristics of various approximate factorizations for the 3D Euler and Navier-Stokes equations are examined using the von-Neumann stability analysis method. Three upwind-difference based factorizations and several central-difference based factorizations are considered for the Euler equations. In the upwind factorizations both the flux-vector splitting methods of Steger and Warming and van Leer are considered. Analysis of the Navier-Stokes equations is performed only on the Beam and Warming central-difference scheme. The range of CFL numbers over which each factorization is stable is presented for one–, two– and three–dimensional flow. Also presented for each factorization is the CFL number at which the maximum eigenvalue is minimized, for all Fourier components, as well as for the high frequency range only. The latter is useful for predicting the effectiveness of multigrid procedures with these schemes as smoothers. Further, local mode analysis is performed to test the suitability of using a uniform flow field in the stability analysis. Some inconsistencies in the results from previous analyses are resolved.

INTRODUCTION

Implicit numerical schemes are gaining increasing popularity since they allow large time steps for advancing the solution of Euler and Navier-Stokes equations to steady state. To reduce the computational cost that is usually involved, the implicit operator is often approximated by a number of smaller easily invertible factors. However, as observed by Thomas et al. [1], the approximately factored scheme has a stability restriction which is more severe in 3D, and also an optimal convergence time step that is not known a priori. Therefore, to avoid the long and costly approach of trial and error of obtaining an optimal CFL number, it is highly desirable to carry out a stability analysis for any numerical scheme. Some researchers have found that analyzing scalar equations such as the convection or the diffusion equation can provide insight into the stability requirements for Euler and Navier-Stokes equations. Beam and Warming [2] employed a combination of these scalar equations to approximate the restriction that will be placed on their ADI methods for compressible Navier-Stokes equations. Jameson and Yoon [3] and Caughey [4], among many others, used the scalar convection equation as a model problem for the Euler equations to investigate appropriate conditions for multigrid implementation. Rather than utilizing model equations, Jespersen and Pulliam [5] developed a technique where Fourier analysis is extended to the actual coupled equations of quasi-one-dimensional Euler equations. Jespersen [6] further extended this technique to 2D Euler equations in order to find the best conditions at which to implement multigrid for a transonic flow. Thomas et al. [1], von Lavante [7] and Anderson et al. [8] have also utilized a similar approach in the stability analysis of Euler equations for certain approximate factorizations and relaxation schemes.

In this paper, the stability analysis for both the Euler and Navier-Stokes equations is carried out for different approximate factorizations. For the Euler equations, three different upwind factorizations, the LU factorization and the Beam and Warming (ADI) factorization are considered while for the Navier-Stokes equations, only the Beam and Warming (ADI) central scheme is analyzed. Also, the quasi-one-dimensional Euler equations investigated by Jespersen and Pulliam [5] is revisited in order to illuminate the actual influence on stability of using approximate Jacobians (to reduce computational costs), instead of the exact Jacobians in upwind factorizations. To ascertain the adequacy of using a uniform flow field in the stability analysis, a local mode analysis is further carried out using actual flow fields (transonic and subsonic) from a quasi-one-dimensional flow.

THEORY AND ANALYSIS

In order to extend the Fourier analysis to the coupled equations under consideration, a discrete analog of these equations is formulated based on different approximate factorizations in this section. The Euler equations are first analyzed using upwind and LU factorizations. The ADI factorization is formulated for the Navier-Stokes equations with the Euler equations as a degenerate case.

Upwind Approximate Factorizations for Euler Equations

The conservation form of the 3–D Euler equations in Cartesian coordinates can be written as:

$$\frac{\partial Q}{\partial t} + \frac{\partial E}{\partial x} + \frac{\partial F}{\partial y} + \frac{\partial G}{\partial z} = 0. \tag{1}$$

where Q is the solution vector and E, F and G are the conserved inviscid fluxes:

$$
\begin{aligned}
Q &= [\rho, \rho u, \rho v, \rho w, \rho e]^T \\
E &= [\rho u, \rho u^2 + p, \rho uv, \rho uw, (\rho e + p)u]^T \\
F &= [\rho v, \rho uv, \rho v^2 + p, \rho vw, (\rho e + p)v]^T \\
G &= [\rho w, \rho wu, \rho wv, \rho w^2 + p, (\rho e + p)w]^T
\end{aligned}
$$

If the Euler implicit scheme is used for time discretization, Eq. (1) can be written in the following form of the augmented Newton's method [9]:

$$
[\mathbf{I} + \Delta t(\delta_x A^n + \delta_y B^n + \delta_z C^n)]\Delta Q^n = -\Delta t(\delta_x E^n + \delta_y F^n + \delta_z G^n) \qquad (3)
$$

where the Jacobians A, B and C are $\frac{\partial E}{\partial Q}$, $\frac{\partial F}{\partial Q}$ and $\frac{\partial G}{\partial Q}$, respectively. The expressions for A, B and C are given in Appendix A.

Flux-vector splitting is employed for the upwind scheme where discretization of the flux derivatives is based on the physical propagation of the solutions of the Euler equations [10]. Based on the direction of the characteristics at a grid point, A, B, C, E, F, etc., are split into their forward and backward contributions. Denoting the forward contribution with "+" and the backward contribution with "-", and forward and backward difference operators with δ_x^+ and δ_x^- respectively, we can rewrite Eq. (3) as:

$$
\begin{aligned}
&[\mathbf{I} + \Delta t(\delta_x^- A^+ + \delta_x^+ A^-) + \Delta t(\delta_y^- B^+ + \delta_y^+ B^-) + \Delta t(\delta_z^- C^+ + \delta_z^+ C^-)]\Delta Q = \\
&\qquad - \Delta t[\delta_x^- E^+ + \delta_x^+ E^- + \delta_y^- F^+ + \delta_y^+ F^- + \delta_z^- G^+ + \delta_z^+ G^-]
\end{aligned} \qquad (4)
$$

The left hand side of the equation is usually approximated with first-order differences, but the right hand side uses second-order differences to improve the overall accuracy of the converged solution. However, even with first-order difference approximations of the implicit terms, the equation is computationally expensive to solve. To reduce this cost, the implicit operator is factored into a sequence of easily invertible terms. Following Anderson et al. [8] we will consider the following three factorizations:

$$\begin{aligned} &[\mathbf{I} + \Delta t(\delta_x^- A^+ + \delta_x^+ A^-)][\mathbf{I} + \Delta t(\delta_y^- B^+ + \delta_y^+ B^-)] \\ &[\mathbf{I} + \Delta t(\delta_z^- C^+ + \delta_z^+ C^-)]\Delta Q^n = -\Delta t R^n \end{aligned} \tag{5}$$

$$\begin{aligned} &[\mathbf{I} + \Delta t(\delta_x^- A^+ + \delta_y^- B^+ + \delta_z^- C^+)] \\ &[\mathbf{I} + \Delta t(\delta_x^+ A^- + \delta_y^+ B^- + \delta_z^+ C^-)]\Delta Q^n = -\Delta t R^n \end{aligned} \tag{6}$$

$$\begin{aligned} &[\mathbf{I} + \Delta t(\delta_x^- A^+ + \delta_x^+ A^- + \delta_z^- C^+)] \\ &[\mathbf{I} + \Delta t(\delta_y^- B^+ + \delta_y^- B^- + \delta_z^+ C^-)]\Delta Q^n = -\Delta t R^n \end{aligned} \tag{7}$$

Eq. (5), (6) and (7) shall be referred to as the spatial, eigenvalue and combination factorizations, respectively.

There are different ways of obtaining the split fluxes expressed in the above equations but two popular methods viz: Steger and Warming flux-vector splitting [11], and van Leer flux-vector splitting [12], are considered in this work.

In the Steger and Warming case, the fluxes are obtained from the following transformation:

$$A^+ = X_A D_A^+ X_A^{-1}, \quad A^- = X_A D_A^- X_A^{-1}, \text{ etc.} \tag{8}$$

where D_A^+ and D_A^- are diagonal matrices whose elements are the positive and negative eigenvalues of A, respectively, and the columns of X_A are the eigenvectors of the Jacobian A. E^+ and E^- are obtained from $E^+ = A^+ Q, \quad E^- = A^- Q$ etc. Eq. (8) gives approximate values for A^+, A^- etc. while exact values can be obtained from:

$$A^+ = \frac{\partial E^+}{\partial Q}, \quad A^- = \frac{\partial E^-}{\partial Q} \tag{9}$$

In order to resolve the singular nature of the Steger and Warming flux-vector splitting at the sonic speed, a, van Leer proposed the following splitting in Cartesian coordinates:

$$E^{\pm} = \pm\frac{\rho(u+a)^2}{4a}\begin{bmatrix} 1 \\ ((\gamma-1)u \pm 2a)/\gamma \\ v \\ w \\ ((\gamma-1)u \pm 2a)^2/2(\gamma^2-1) + \frac{1}{2}(v^2+w^2) \end{bmatrix} \tag{10}$$

With similar forms for F^+, F^-, G^+, G^-, the Jacobians A^+, A^- etc. are obtained from Eq. (9). The analytical expressions for these can be obtained using a symbolic manipulator such as Mathematica. In these expressions, van Leer ensured continuous differentiability of the fluxes especially at the sonic transition [10].

LU Approximate Factorization for Euler Equations

This approach has become popular in recent times. It factors the implicit term of Eq. (3) into two components such that each component is strictly either a lower (L) or an upper (U) matrix as in the following equation:

$$\begin{aligned} [\mathbf{I} + \Delta t(\delta_x^- A_1 + \delta_y^- B_1 + \delta_z^- C_1)][\mathbf{I} + \Delta t(\delta_x^+ A_2 + \delta_y^+ B_2 + \delta_z^+ C_2)]\Delta Q^n = \\ -\Delta t(\delta_x E + \delta_y F + \delta_z G) \end{aligned} \tag{11}$$

The Jacobian matrices are split to ensure diagonal dominance for each matrix inversion at each grid point. For our numerical computation we have adopted the flux-vector splitting devised by Jameson and Turkel [13].

$$A_1 = \frac{(A + r_A \mathbf{I})}{2}, \qquad A_2 = \frac{(A - r_A \mathbf{I})}{2}, \quad \text{etc.} \tag{12}$$

where $r_A \geq \max(|\lambda_A|)$, etc. and λ_A are the eigenvalues of matrix A viz: $u+a, u-a, u, u, u$.

The explicit terms are central differenced and it is necessary to damp the associated high frequency waves and/or to correct the odd-even decouplings. In this study, the following combination of second- and fourth-order explicit linear dissipations is employed. According to Caughey [4], and Yokota and Caughey [14], the former term is necessary for any spurious waves at the vicinity of shock while the latter ensures convergence to steady state.

$$D_x^e = \kappa_2 \Delta t \Delta x \delta_{xx} - \kappa_4 \Delta t \Delta x^3 \delta_{xxxx} \tag{13}$$

Noting that $\delta_{xx} = \frac{1}{\Delta x}(\delta_x^+ - \delta_x^-)$, the second-order term is split in a manner consistent with the differencing of the Jacobians and is implemented implicitly. Thus, with similar terms in the y- and z-directions, we write:

$$\begin{gathered}[\mathbf{I} + \Delta t(\delta_x^- A_1 + \delta_y^- B_1 + \delta_z^- C_1) + \kappa_2 \Delta t(\delta_x^- + \delta_y^- + \delta_z^-)] \\ [\mathbf{I} + \Delta t(\delta_x^+ A_2 + \delta_y^+ B_2 + \delta_z^+ C_2) - \kappa_2 \Delta t(\delta_x^+ + \delta_y^+ + \delta_z^+)]\Delta Q^n = \\ -\Delta t(\delta_x E + \delta_y F + \delta_z G) - \kappa_4 \Delta t(\Delta x^3 \delta_{xxxx} + \Delta y^3 \delta_{yyyy} + \Delta z^3 \delta_{zzzz})\mathbf{I}Q\end{gathered} \tag{14}$$

This factorization is similar to the eigenvalue factorization (see Eq. (6)) except that the explicit terms are centrally differenced rather than upwinded, thus, requiring the addition of dissipation. Also, the split fluxes of Jameson and Turkel which are less difficult to derive are used to achieve diagonal dominance in this case.

ADI Factorizations for Euler and Navier-Stokes Equations

The 3–D Navier-Stokes equations in Cartesian coordinates can be written as:

$$\frac{\partial Q}{\partial t} + \frac{\partial(E - E_v)}{\partial x} + \frac{\partial(F - F_v)}{\partial y} + \frac{\partial(G - G_v)}{\partial z} = 0 \tag{15}$$

where E, F and G are as defined earlier, and E_v, F_v, and G_v are the viscous fluxes:

$$E_v = \begin{bmatrix} 0 \\ \frac{2}{3}\mu(2u_x - v_y - w_z) \\ \mu(u_y + v_x) \\ \mu(u_z + w_x) \\ \mu v(u_y + v_x) + \mu w(u_z + w_x) + \\ \frac{2}{3}\mu u(2u_x - v_y - w_z) + kT_x \end{bmatrix} \tag{16}$$

$$F_v = \begin{bmatrix} 0 \\ \mu(u_y + v_x) \\ \frac{2}{3}\mu(2v_y - u_x - w_z) \\ \mu(v_z + w_y) \\ \mu u(u_y + v_x) + \mu w(v_z + w_y) + \\ \frac{2}{3}\mu v(2v_y - u_x - w_z) + kT_y \end{bmatrix} \tag{17}$$

$$G_v = \begin{bmatrix} 0 \\ \mu(w_x + u_z) \\ \mu(v_z + w_y) \\ \frac{2}{3}\mu(2w_z - v_y - u_x) \\ \mu u(w_x + u_z) + \mu v(v_z + w_y) + \\ \frac{2}{3}\mu w(2w_z - v_y - u_x) + kT_z \end{bmatrix} \tag{18}$$

Where $T = \frac{p}{\rho c_v(\gamma-1)}$ and p is as defined in Appendix A. Also, Stokes hypothesis ($\lambda = -\frac{2}{3}\mu$) has been assumed. With E_v, F_v and G_v set to zero, we recover the Euler Eqs. (1).

Following the approach of Beam and Warming [9], the viscous fluxes are split directionally. Also following the approach presented in Anderson et al. [14] for 2D Navier-Stokes equations, analysis yields the following ADI approximate factorization for the 3D Navier-Stokes equations, while assuming Euler implicit time integration and constant fluid properties:

$$[\mathbf{I} + \Delta t(\delta_x A - \delta_{xx} R)][\mathbf{I} + \Delta t(\delta_y B - \delta_{yy} S)][\mathbf{I} + \Delta t(\delta_z C - \delta_{zz} Y)]\Delta Q^n =$$
$$-\Delta t[A\delta_x - R\delta_{xx} - R_1\delta_{yx} - R_2\delta_{zx} + B\delta_y - S_1\delta_{xy} - S\delta_{yy} - S_2\delta_{zy} +$$
$$C\delta_z - Y_1\delta_{xz} - Y_2\delta_{yz} - Y\delta_{zz}]Q \tag{19}$$

The analytical expressions for the various Jacobians (from the viscous fluxes) that appear in this equation are shown in Appendix B. The right-hand-side resulted from linearization and from assuming the flux Jacobians locally constant.

To damp the high frequency waves that will arise due to central differencing, second-order implicit ($D_x^i = -\varepsilon_i \Delta t \Delta x \delta_{xx}$) and fourth-order explicit ($D_x^e = -\varepsilon_e \Delta t \Delta x^3 \delta_{xxxx}$) artificial dissipations are added in the numerical examples. Thus, with similar dissipations added in the y- and z-directions Eq. (19) becomes:

$$[\mathbf{I} + \Delta t(\delta_x A - \delta_{xx} R) - \varepsilon_i \Delta t \Delta x \delta_{xx} \mathbf{I}][\mathbf{I} + \Delta t(\delta_y B - \delta_{yy} S) - \varepsilon_i \Delta t \Delta y \delta_{yy} \mathbf{I}]$$
$$[\mathbf{I} + \Delta t(\delta_z C - \delta_{zz} Y) - \varepsilon_i \Delta t \Delta z \delta_{zz} \mathbf{I}]\Delta Q^n \quad =$$
$$- \Delta t[A\delta_x - R\delta_{xx} - R_1\delta_{yx} - R_2\delta_{zx} + B\delta_y - S_1\delta_{xy} - S\delta_{yy} - S_2\delta_{zy} + C\delta_z$$
$$- Y_1\delta_{xz} - Y_2\delta_{yz} - Y\delta_{zz} + (\varepsilon_e \Delta x^3 \delta_{xxxx} + \varepsilon_e \Delta y^3 \delta_{yyyy} + \varepsilon_e \Delta z^3 \delta_{zzzz})\mathbf{I}]Q \tag{20}$$

The corresponding factorization for the Euler equations is obtained by setting to zero the viscous flux Jacobians $R, R_1, R_2, S, S_1, S_2, Y, Y_1, Y_2$.

In the forgone analyses, different approximate factorizations that are widely used in practice have been formulated for the 3D Euler and Navier-Stokes equations. The convergence characteristics of each of these are examined using the von-Neumann type Fourier analysis methods.

von-Neumann Stability Analysis

Each of Eqs. (5), (6), (7), (14) and (20) can be expressed as

$$N\Delta Q^n = -L = -\Delta t R^n \tag{21}$$

von-Neumann stability analysis is used on this system of linear Eq. (21) by letting the step by step solution be characterized by

$$Q^n = \lambda^n U_0 e^{Ii\phi_x} e^{Ij\phi_y} e^{Ik\phi_z} \tag{22}$$

where $I = \sqrt{-1}$, λ is the amplification factor and ϕ_x, ϕ_y, ϕ_z represent the modes in the x-, y- and z-directions. Thus, Eq. (14) reduces to a complex generalized eigenvalue problem of the form [5]:

$$\hat{\mathrm{K}}\mathrm{v} = \lambda \hat{\mathrm{N}}\mathrm{v} \quad \text{where } \hat{\mathrm{K}} = \hat{\mathrm{N}} - \hat{\mathrm{L}} \tag{23}$$

The Fourier symbols $\hat{N}$and $\hat{L}$ are derived for each of the factorizations shown in Eq. (5), (6), (7), (14) and (20). For example, for the spatial factorization (represented by Eq (5)), employing a first-order differencing for the implicit operator and second-order differencing for the explicit operator, these two Fourier symbols are expressed as follows:

$$\begin{aligned}\hat{N} = &\left\{\mathbf{I} + \frac{\Delta t}{\Delta x}\left[(A^+ - A^-)(1 - \cos\phi_x) + (A^+ + A^-)I\sin\phi_x\right]\right\} \\ &\left\{\mathbf{I} + \frac{\Delta t}{\Delta y}\left[(B^+ - B^-)(1 - \cos\phi_y) + (B^+ + B^-)I\sin\phi_y\right]\right\} \\ &\left\{\mathbf{I} + \frac{\Delta t}{\Delta z}\left[(C^+ - C^-)(1 - \cos\phi_z) + (C^+ + C^-)I\sin\phi_z\right]\right\}\end{aligned} \tag{24}$$

$$\begin{aligned}\hat{L} = &\frac{\Delta t}{2\Delta x}\left[(A^+ - A^-)(3 + \cos 2\phi_x - 4\cos\phi_x) + (A^+ + A^-)(4\sin\phi_x - \sin 2\phi_x)I\right] \\ &+\frac{\Delta t}{2\Delta y}\left[(B^+ - B^-)(3 + \cos 2\phi_y - 4\cos\phi_y) + (B^+ + B^-)(4\sin\phi_y - \sin 2\phi_y)I\right] \\ &+\frac{\Delta t}{2\Delta z}\left[(C^+ - C^-)(3 + \cos 2\phi_z - 4\cos\phi_z) + (C^+ + C^-)(4\sin\phi_z - \sin 2\phi_z)I\right]\end{aligned} \tag{25}$$

The Fourier symbols corresponding to the other approximate factorizations are documented in Demuren and Ibraheem [16].

SOLUTION PROCEDURE

The convergence characteristics for solution algorithms based on each of the factorizations discussed are investigated by solving the generalized eigenvalue problem (23) over a fixed number of Fourier modes. 16 modes are selected, in the range $0 \leq \phi_x, \phi_y, \phi_z \leq 2\pi$, and over these modes the maximum eigenvalue ($\lambda_{\max}$), the average eigenvalue (λ_{avg}) and the smoothing factor (λ_μ) are computed. The smoothing factor is computed to show the effectiveness of the selected scheme as a relaxation operator in a multigrid implementation. This is calculated from $\lambda_\mu = \max(|\lambda|)$ for the high frequency modes in the range $\frac{\pi}{2} \leq \phi_x, \phi_y, \phi_z \leq \frac{3\pi}{2}$. For the analyses, uniform flow is assumed with $M_\infty = 0.8$, zero yaw and angle of attack and $\gamma = 1.4$. Further, the grid spacing is assumed to be uniform in all directions. The time step, Δt is calculated from:

$$\Delta t = \frac{CFL}{\left[\frac{|u|}{\Delta x} + \frac{|v|}{\Delta y} + \frac{|w|}{\Delta z} + a\sqrt{\frac{1}{\Delta x^2} + \frac{1}{\Delta y^2} + \frac{1}{\Delta z^2}}\right]} \tag{26}$$

As a further test case, quasi-one-dimensional Euler equations are solved with a similar formulation as the 3–D upwind spatial factorization, with uniform conditions of $M_\infty = 0.5$, zero yaw and angle of attack and $\rho = 1.0$, chosen to enable comparison with Jespersen and Pulliam's results [5]. In this case, the computed parameters are the maximum eigenvalue ($\lambda_{\max}$), the L2–norm of the eigenvalue (l_2) and the eigenvalue at $\phi_x = \pi$ (λ_π).

RESULTS AND DISCUSSIONS

Computed values of the maximum eigenvalue ($\lambda_{\mathbf{max}}$), the average eigenvalue ($\lambda_{\mathbf{avg}}$) and the smoothing factor (λ_{μ}) for the spatial, eigenvalue and combination factorizations based on the Steger and Warming flux-vector splitting are shown in Figs. (1a), (1b) and (1c) respectively. Both the eigenvalue and the combination factorizations are unconditionally stable for all CFL numbers. The spatial factorization is stable only for CFL numbers below 5. The maximum eigenvalue for each of the spatial, eigenvalue and combination factorizations is minimized at CFL numbers of 3, 8 and 7, respectively. Corresponding results obtained for 2–D case (not shown) indicate that the spatial and eigenvalue factorizations are unconditionally stable and have lower ($\lambda_{\mathbf{max}}$) than the 3D case, for all CFL numbers. The corresponding minimum value of ($\lambda_{\mathbf{max}}$) are minimized at a CFL numbers of 8 and 10, respectively. The 1–D case is also stable for all CFL numbers with the maximum eigenvalue minimized at a CFL number of 11, for both spatial and eigenvalue factorizations (Table I).

Figs. (2a), (2b) and (2c) show the convergence characteristics of each of the factorizations based on the van Leer flux-vector splitting. These agree very well with that of Anderson et al. [8]. Except for the spatial factorization, all the schemes are unconditionally stable for all CFL numbers. The spatial factorization is stable only for CFL number below 14. The maximum eigenvalues for the spatial, eigenvalue and combination factorizations are minimized at CFL numbers of 7, 4 and 7 respectively. From the λ_{μ} curve, it appears that the spatial factorization with the Steger and Warming method has poorer smoothing properties comparison with the van Leer spatial factorization. Based on linear analysis, there is also a smaller range of CFL numbers over which it is stable. The spatial factorization and the eigenvalue factorization of the 2–D case are found to be unconditionally stable with maximum eigenvalue minimized at CFL numbers of about 9 and 6, respectively. Results for the 1–D case are almost identical to those of the Steger and Warming analysis, with maximum eigenvalues minimized at CFL numbers of 11 and 19, respectively.

In the computations presented thus far, approximate Jacobians derived from a time linearization of the Euler equations have been employed in the Steger and Warming method on both the implicit and explicit sides. The effect of using the exact Jacobians in the stability analysis was investigated with 1D Euler equations using uniform conditions of $M_\infty = 0.5$ and $\rho = 1.0$. The results are compared in Figs. (3a) and (3b), respectively. In both cases, first-order differencing were used on the implicit side and second-order differencing on the explicit side, as in previous computations. From these figures, it can be observed that the results (as reflected by the variation of $\lambda_{\mathbf{max}}, \lambda_{\mathbf{avg}}, \lambda_\mu$ with CFL) are similar. This shows that the use of approximate Jacobians does not place a restriction on the stability. This is at variance with the conclusion of Jespersen and Pulliam [5]. Restriction on the stability will result if the Jacobians are "mixed" such that approximate Jacobians are used on the implicit side and the exact Jacobians on the explicit side. In this case, Fig. (3c) shows that the stability is restricted to CFL numbers below 1. On the other hand, if the Jacobians are mixed in the reverse order i.e., with exact Jacobians on the implicit side and approximate Jacobians on the explicit side, the results (see Fig. (3d)) is not significantly affected. Further, from Figs. (4a), (4b), (4c) and (4d), where we have used second-order differencing on both sides, similar conclusions can be drawn.

All computations have been based on uniform flow conditions. To ascertain the suitability of using such uniform flow field assumptions in the stability analysis, computations were carried out on two non-uniform flow fields with quasi-1D Euler equations using local mode analysis. These correspond to supersonic and transonic flows in a converging duct with steady-state solutions shown in Figs. (5a) and (5b), respectively. The von-Neumann method is applied at each point in the flow field thereby accounting for the variation in flow properties. The stability results for the supersonic case for both first-order and second-order differencing of the implicit side are shown in Figs. (5c) and (5d). Corresponding results for the transonic case are shown in Figs. (5e) and (5f). These results follow a similar trend as those obtained for 1D Euler equations with uniform flow properties, except that instability is now predicted for lower CFL numbers. Boundary conditions were implemented explicitly and might have contributed to this instability. The use of local mode analysis here, is similar to the use of the total matrix method approach of Jespersen and Pulliam [5], except that, the former is easier to compute because it involves the solution of only a 3X3 eigenvalue problem.

Figs. (6a), (6b) and (6c) show the convergence characteristics of the 3D Euler equations using the LU approximate factorization with central difference approximations and various levels of second- and fourth-order artificial viscosities; κ_2 and κ_4. Without the addition of second-order dissipation i.e., $\kappa_2 = 0$, the coefficient $\kappa_4 = 0.4$ yields the optimal results (see Fig. (6a)). Appropriate combinations of κ_2 and κ_4 (especially, when $\kappa_4 \geq \kappa_2$) considerably reduce the amplification factor (see Fig. (6b) as compared with Fig. (6c)). The amplification factor is minimized in each case at a CFL of about 5. Similar trends were observed in 1D and 2D cases.

In Figs. (7a), (7b), (7c), (8a), (8b) and (8c), the convergence characteristics for the full 3–D Naiver-Stokes equations using the Beam and Warming (ADI) central difference scheme as the baseline solution algorithm are shown for different Reynolds numbers and levels of artificial dissipation. For Reynolds number of 100 (Fig. 7a) and with no dissipation added, the scheme is stable for CFL number below 18. However, with artificial dissipation coefficients of $\varepsilon_e = 0.5$ and $\varepsilon_i = 1.0$ (Fig. 7b), the stability is restricted to a lower CFL number of 10, but with better smoothing properties. Optimal dissipation coefficients of $\varepsilon_e = 1.0$ and $\varepsilon_i = 2.0$ (Fig. 7c), are found to improve the stability to a CFL of about 18 while maintaining good smoothing properties. The maximum eigenvalue is minimized at a CFL number of about 4 for this optimal dissipation. Both 1–D and 2–D cases are unconditionally stable for all levels of dissipation. For $\varepsilon_e = 1.0$ and $\varepsilon_i = 2.0$, their maximum eigenvalues are both minimized at about CFL numbers of 24 and 11, respectively. For Reynolds number of 10^6, the results are similar to the cases with Reynolds number of 100, especially when dissipation is added. Hence, the stability results are not significantly affected by Reynolds number. Figs. (9a), (9b) and (9c) show the stability results for Euler equations with the Beam and Warming (ADI) central difference scheme. These results are identical to those obtained for the full Navier-Stokes equations at a Reynolds number of 10^6. Generally, the addition of dissipation reduces the amplification factor and the smoothing factor at lower CFL numbers. Optimal smoothing is usually at a CFL number close to 1.

The above results are summarised in Table I. In the Table, λ_m stands for the minimum amplification factor, CFL_m for the corresponding CFL number, CFL_l the maximum CFL number for stability and CFL_μ is the CFL number at which λ_μ is minimized.

CONCLUSIONS

The stability of some approximate factorization schemes for the solution of the 3D Euler equations and Navier-Stokes equations have been studied. For the Euler equations, the Steger and Warming, and van Leer flux-vector splittings were used with three different upwind factorizations namely: spatial, eigenvalue and combination factorizations. For both flux-vector splittings, the eigenvalue and combination factorizations are unconditionally stable, but the spatial factorization is only conditionally stable for CFL numbers below 5 for the Steger and Warming scheme, and 14 for the van Leer scheme. Moreover, the amplification factor (λ_{max}) is minimized for the Steger and Warming scheme at CFL numbers of 3, 7, and 8 respectively, and for the van Leer scheme at 7, 4, and 7, for spatial, eigenvalue and combination factorizations, respectively. Each of the approximate factorization methods has good smoothing properties for the van Leer flux-vector splitting, while for the Steger and Warming splitting, the smoothing factors are comparatively worse. Therefore, the van Leer splitting will be preferable for multigrid implementation. The Euler equations have also been analyzed for stability using the LU approximate factorization with central differences and various levels of artificial dissipation. It was found to be unconditionally stable in all dimensions with the maximum eigenvalue minimized at a CFL number of about 3. Contrary to the conclusion drawn by Jespersen and Pulliam [5] that the use of approximate Jacobians places restriction on the stability, it is shown, after careful investigation, that if they are used on both the implicit and the explicit sides, the stability results are comparable to the case where the exact Jacobians are used. The von-Neumann analysis method was also employed in performing local mode analysis for actual (supersonic and transonic) flow fields of a quasi 1D problem to show the suitability of using uniform flow field in the stability analysis. Stability results for the 3D Euler and Navier-Stokes equations solved with the Beam and Warming (ADI) central scheme with various levels of artificial dissipation (and at different Reynolds number for the latter) have been presented. It was observed that the stability is not significantly affected by Reynolds numbers and that addition of dissipation reduces the amplification factor and the smoothing factor at lower CFL numbers.

ACKNOWLEDGEMENT

This work is funded by NASA Lewis Research Center under Grant No. NAG-3–1329 with Dr. James Scott as Technical Monitor. Part of it was also conducted at ICOMP, NASA Lewis Research Center. Computations were performed on supercomputers at NASA Lewis and NASA Ames Research Centers.

APPENDIX A

Inviscid Flux Jacobians

$$A = \begin{bmatrix} 0 & 1 & 0 & 0 & 0 \\ -u^2 + \frac{\gamma-1}{2}q^2 & (3-\gamma)u & -(\gamma-1)v & -(\gamma-1)w & (\gamma-1) \\ -uv & v & u & 0 & 0 \\ -uw & w & 0 & u & 0 \\ -u\left[\gamma e - (\gamma-1)q^2\right] & \gamma e - \frac{\gamma-1}{2}\left(q^2 + 2u^2\right) & -(\gamma-1)uv & -(\gamma-1)uw & \gamma u \end{bmatrix}$$

$$B = \begin{bmatrix} 0 & 0 & 1 & 0 & 0 \\ -uv & v & u & 0 & 0 \\ -v^2 + \frac{\gamma-1}{2}q^2 & -(\gamma-1)u & (3-\gamma)v & -(\gamma-1)w & (\gamma-1) \\ -uw & 0 & w & u & 0 \\ -v\left[\gamma e - (\gamma-1)q^2\right] & -(\gamma-1)uv & \gamma e - \frac{(\gamma-1)}{2}\left(q^2 + 2v^2\right) & -(\gamma-1)vw & \gamma v \end{bmatrix}$$

$$C = \begin{bmatrix} 0 & 0 & 0 & 1 & 0 \\ -uw & w & 0 & u & 0 \\ -vw & 0 & w & v & 0 \\ -w^2 + \frac{\gamma-1}{2}q^2 & -(\gamma-1)u & -(\gamma-1)v & (3-\gamma)w & (\gamma-1) \\ -w\left[\gamma e - (\gamma-1)q^2\right] & -(\gamma-1)uw & -(\gamma-1)uw & \gamma e - \frac{(\gamma-1)}{2}\left(q^2 + 2w^2\right)u & \gamma u \end{bmatrix}$$

where $p = (\gamma-1)\left(\rho e - 0.5q^2\right)$ and $q^2 = u^2 + v^2 + w^2$

APPENDIX B

Viscous Flux Jacobians

$$R = \frac{\partial E_{v,x}}{\partial Q_x} = \tfrac{\mu}{\rho}\begin{bmatrix} 0 & 0 & 0 & 0 & 0 \\ -\frac{4}{3}u & \frac{4}{3} & 0 & 0 & 0 \\ -v & 0 & 1 & 0 & 0 \\ -w & 0 & 0 & 1 & 0 \\ \frac{\gamma}{Pr}(q^2-e)-\left(\frac{4}{3}u^2-v^2-w^2\right) & u\left(\frac{4}{3}-\frac{\gamma}{Pr}\right) & v\left(1-\frac{\gamma}{Pr}\right) & w\left(1-\frac{\gamma}{Pr}\right) & \frac{\gamma}{Pr} \end{bmatrix}$$

$$S = \frac{\partial F_{v,y}}{\partial Q_y} = \tfrac{\mu}{\rho}\begin{bmatrix} 0 & 0 & 0 & 0 & 0 \\ -u & 1 & 0 & 0 & 0 \\ -\frac{4}{3}v & 0 & \frac{4}{3} & 0 & 0 \\ -w & 0 & 0 & 1 & 0 \\ \frac{\gamma}{Pr}(q^2-e)-\left(\frac{4}{3}v^2-u^2-w^2\right) & u\left(1-\frac{\gamma}{Pr}\right) & v\left(\frac{4}{3}-\frac{\gamma}{Pr}\right) & w\left(1-\frac{\gamma}{Pr}\right) & \frac{\gamma}{Pr} \end{bmatrix}$$

$$Y = \frac{\partial G_{v,z}}{\partial Q_z} = \tfrac{\mu}{\rho}\begin{bmatrix} 0 & 0 & 0 & 0 & 0 \\ -u & 1 & 0 & 0 & 0 \\ -v & 0 & 1 & 0 & 0 \\ -\frac{4}{3}w & 0 & 0 & \frac{4}{3} & 0 \\ \frac{\gamma}{Pr}(q^2-e)-\left(\frac{4}{3}w^2-u^2-v^2\right) & u\left(1-\frac{\gamma}{Pr}\right) & v\left(1-\frac{\gamma}{Pr}\right) & w\left(\frac{4}{3}-\frac{\gamma}{Pr}\right) & \frac{\gamma}{Pr} \end{bmatrix}$$

$$R_1 = \frac{\partial E_{v,y}}{\partial Q_y} = \tfrac{\mu}{\rho}\begin{bmatrix} 0 & 0 & 0 & 0 & 0 \\ -\frac{2}{3}v & 0 & -\frac{2}{3} & 0 & 0 \\ -u & 1 & 0 & 0 & 0 \\ 0 & 0 & 0 & 0 & 0 \\ -\frac{1}{3}uv & v & -\frac{2}{3}u & 0 & 0 \end{bmatrix}, R_2 = \frac{\partial E_{v,z}}{\partial Q_z} = \tfrac{\mu}{\rho}\begin{bmatrix} 0 & 0 & 0 & 0 & 0 \\ \frac{2}{3}w & 0 & 0 & -\frac{2}{3} & 0 \\ 0 & 0 & 0 & 0 & 0 \\ -u & 1 & 0 & 0 & 0 \\ -\frac{1}{3}uw & w & 0 & -\frac{2}{3}u & 0 \end{bmatrix}$$

$$S_1 = \frac{\partial F_{v,x}}{\partial Q_x} = \tfrac{\mu}{\rho}\begin{bmatrix} 0 & 0 & 0 & 0 & 0 \\ -v & 0 & 1 & 0 & 0 \\ -\frac{2}{3}u & -\frac{2}{3} & 0 & 0 & 0 \\ 0 & 0 & 0 & 0 & 0 \\ -\frac{1}{3}uv & -\frac{2}{3}v & u & 0 & 0 \end{bmatrix}, S_2 = \frac{\partial F_{v,z}}{\partial Q_z} = \tfrac{\mu}{\rho}\begin{bmatrix} 0 & 0 & 0 & 0 & 0 \\ 0 & 0 & 0 & 0 & 0 \\ \frac{2}{3}w & 0 & 0 & -\frac{2}{3} & 0 \\ -v & 0 & 1 & 0 & 0 \\ -\frac{1}{3}uv & 0 & w & -\frac{2}{3}v & 0 \end{bmatrix}$$

$$Y_1 = \frac{\partial G_{v,x}}{\partial Q_x} = \tfrac{\mu}{\rho} \begin{bmatrix} 0 & 0 & 0 & 0 & 0 \\ -w & 0 & 0 & 1 & 0 \\ 0 & 0 & 0 & 0 & 0 \\ \frac{2}{3}u & -\frac{2}{3} & 0 & 0 & 0 \\ -\frac{1}{3}uw & -\frac{2}{3}w & 0 & u & 0 \end{bmatrix}, Y_2 = \frac{\partial G_{v,y}}{\partial Q_y} = \tfrac{\mu}{\rho} \begin{bmatrix} 0 & 0 & 0 & 0 & 0 \\ 0 & 0 & 0 & 0 & 0 \\ -w & 0 & 0 & 1 & 0 \\ \frac{2}{3}v & 0 & -\frac{2}{3} & 0 & 0 \\ -\frac{1}{3}vw & 0 & -\frac{2}{3}w & v & 0 \end{bmatrix}$$

where $Pr = \frac{\mu c_p}{k} = \frac{\mu \gamma c_v}{k}$.

REFERENCES

[1] J. L. Thomas, B. van Leer and R. W. Walters, Implicit Flux-Split Scheme For the Euler Equations, AIAA paper 85-1680, 1985.

[2] R. M. Beam and R. F. Warming, An Implicit Scheme for the Compressible Navier-Stokes Equations, AIAA J., vol. 16, pp. 393–402, 1978.

[3] A. Jameson and S. Yoon, Multigrid Solution of the Euler Equations using Implicit Schemes, AIAA paper 85–0293, 1985.

[4] D. A. Caughey, Diagonal Implicit Multigrid Algorithm for the Euler Equations, AIAA J., vol. 26, pp. 841–850, 1988.

[5] D. C. Jespersen and T. H. Pulliam, Flux Vector Splitting and Approximate Newton Methods, AIAA Sixth CFD Conference, 1983.

[6] D. C. Jespersen, Design and Implementation of a Multigrid Code for the Euler Equations, Applied Mathematics and Computation, vol. 13, pp. 357–374, 1983.

[7] E. von Lavante, D. Claes and W. K. Anderson, The Effects of various Implicit operators on a Flux Vector Splitting Method, AIAA paper 86–0273, 1986.

[8] W. K. Anderson, J. L. Thomas and D. L. Whitfield, Three-Dimensional Multigrid Algorithms for the Flux-Split Euler Equations, NASA Technical Paper 2829, 1988.

[9] C. A. J. Fletcher, Computational Techniques For Fluid Dynamics 2, chap. 14, Springer-Verlag, New York, 1991.

[10] C. Hirsch, Numerical Computation of Internal and External Flows 2, chap. 20, John Wiley & Sons, New York, 1990.

[11] J. L. Steger and R. F. Warming, Flux Vector Splitting of the Inviscid Gas-dynamic Equations with Application to Finite-Difference Methods, J. of Comp. Physics, vol. 40, pp. 263–293, 1980.

[12] B. van Leer, Flux-Vector Splitting For the Euler Equations, ICASE Report No. 82-30, 1982.

[13] A. Jameson and E. Turkel, Implicit Schemes and LU Decompositions, Mathematics of Computaion, vol. 37, pp. 385-397, 1981.

[14] J. W. Yokota and A. D. Caughey, LU Implicit Multigrid Algorithm for the Three-Dimensional Euler Equations, AIAA J., vol. 26, pp. 1061-1069, 1988.

[15] D. A. Anderson, J. C. Tannehill and R. H. Pletcher, Computational Fluid Mechanics and Heat Transfer, chap. 9, McGraw Hill, New York, 1984.

[16] A. O. Demuren and S. O. Ibraheem, Convergence Acceleration of the Proteus Computer Code With Multigrid Methods, Interim Report Prepared for the Internal Fluid Mechanics Division, NASA Lewis Research Center, 1992.

TABLE I: STABILITY ANALYSIS RESULTS FOR VARIOUS FACTORIZATIONS

Factorization or Dissipation Coefficients		1D λ_m	1D CFL_m	1D CFL_l	1D CFL_μ	2D λ_m	2D CFL_m	2D CFL_l	2D CFL_μ	3D λ_m	3D CFL_m	3D CFL_l	3D CFL_μ
Spatial	Steger/Warming	.91	11	-	3	.90	8	-	7	.97	3	5	3
	van Leer	.91	11	-	3	.88	9	-	4	.92	7	14	3
Eigenvalue	Steger/Warming	.91	11	-	3	.88	10	-	7	.91	7	-	6
	van Leer	.83	19	-	7	.93	6	-	3	.96	4	-	3
Combination	Steger/Warming	-	-	-	-	-	-	-	-	.90	8	-	7
	van Leer	-	-	-	-	-	-	-	-	.91	7	-	4
LU	$\kappa_2=0,\ \kappa_4=.4$	.98	5	-	1	.97	4	-	1	.97	3	-	1
	$\kappa_2=2,\ \kappa_4=3$	.93	4	-	2	.92	3	-	2	.91	3	-	2
	$\kappa_2=3,\ \kappa_4=2$	.96	4	-	1	.95	3	-	1	.95	3	-	1
ADI Navier-Stokes $Re=10^2$	$\epsilon_2=0,\ \epsilon_4=0$	-	-	-	-	.93	9	-	6	.95	7	18	5
	$\epsilon_2=1,\ \epsilon_4=.5$	.94	24	-	1	.90	13	-	1	.96	6	10	1
	$\epsilon_2=2,\ \epsilon_4=1$	.96	24	-	1	.93	11	-	1	.98	4	18	1
ADI* Navier-Stokes $Re=10^6$	$\epsilon_2=0,\ \epsilon_4=0$	-	-	-	-	.93	8	-	8	.97	8	16	1
	$\epsilon_2=1,\ \epsilon_4=.5$	.94	23	-	1	.91	13	-	1	.96	6	10	1
	$\epsilon_2=2,\ \epsilon_4=1$	.96	24	-	1	.93	12	-	1	.97	4	18	1

* Results for the ADI Euler Equations are identical.

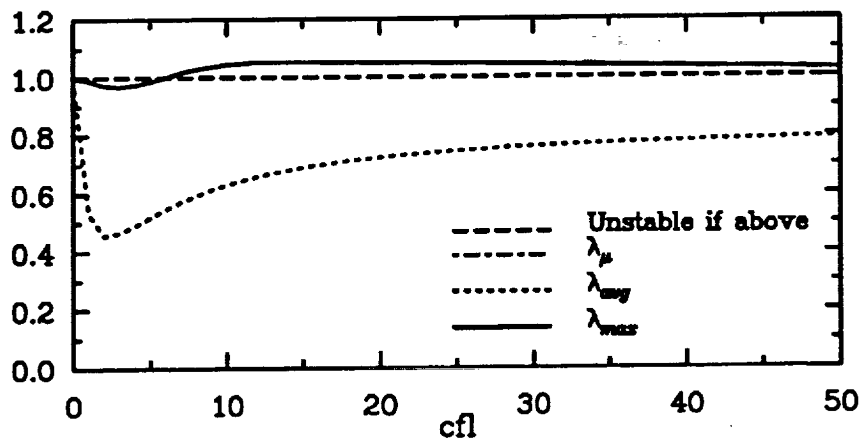

(a) Spatial Factorization

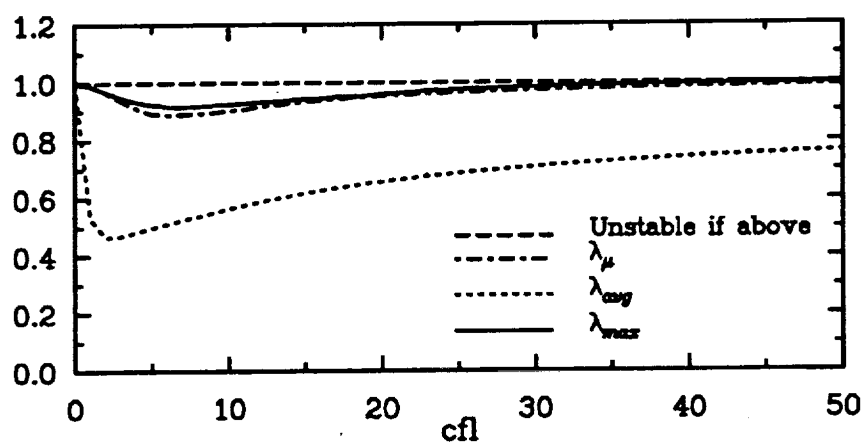

(b) Eigenvalue Factorization

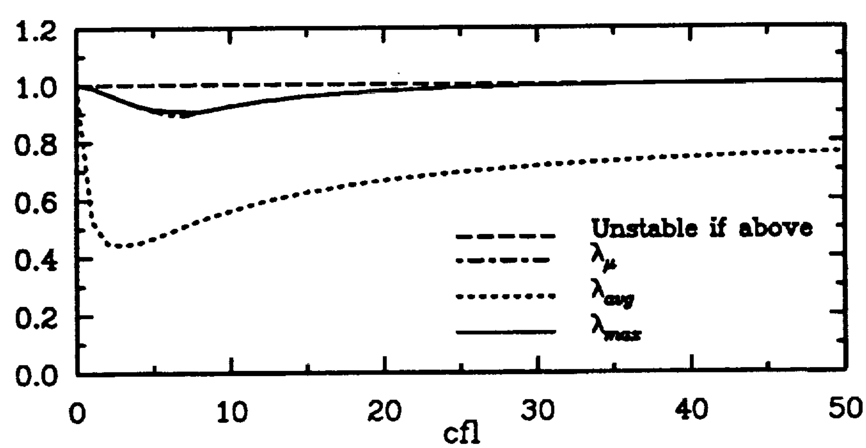

(c) Combination Factorization

Figs. (1a)–(1c): Eigenvalue for Linear Stability Analysis of 3–D Euler Equations (Steger & Warming's Upwind Factorization)

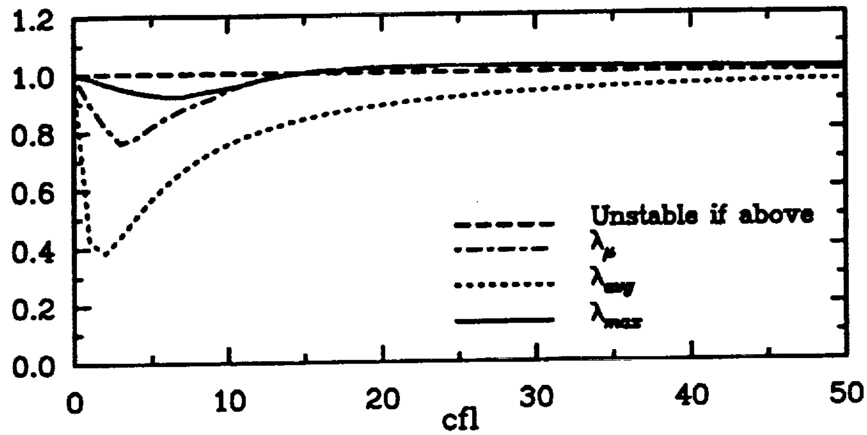

(a) Spatial Factorization

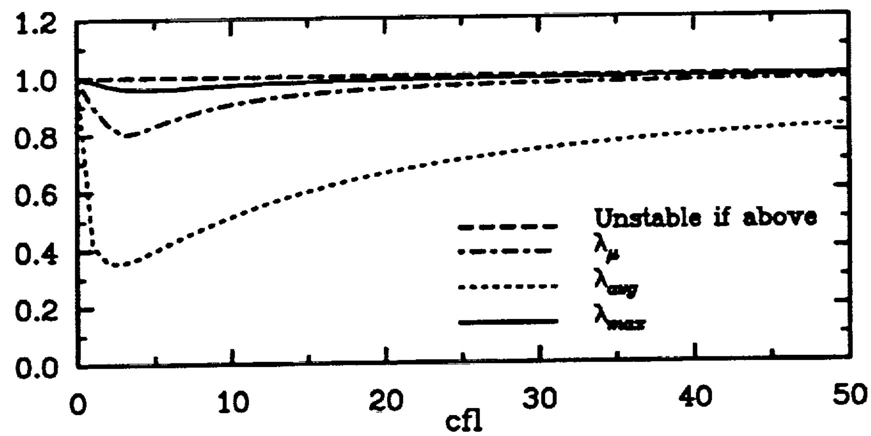

(b) Eigenvalue Factorization

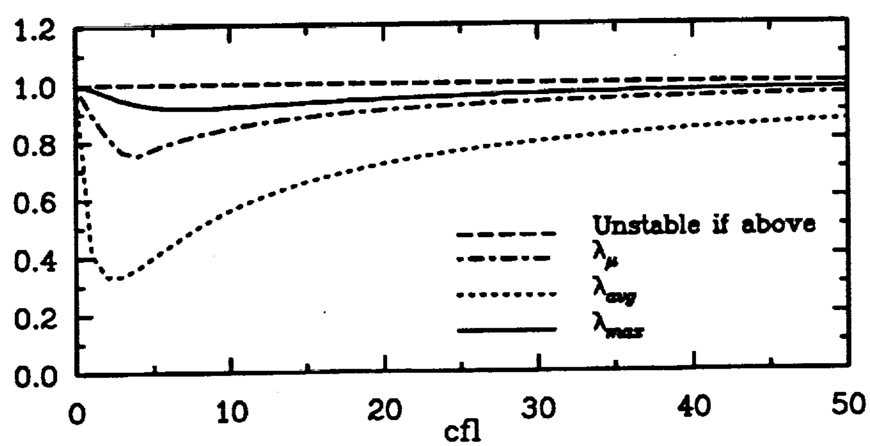

(c) Combination Factorization

Figs. (2a)–(2c): Eigenvalues for Linear Stability Analysis of 3–D Euler Equations (van Leer's Upwind Factorization)

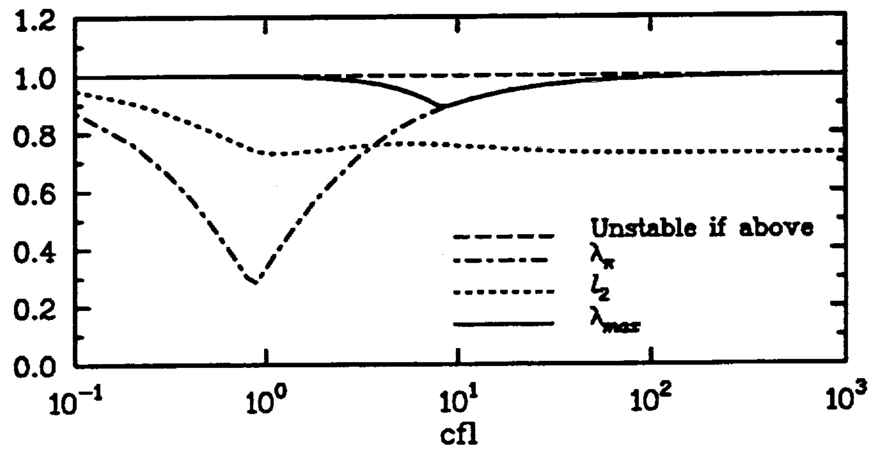

(a) Approx. Jacobians (lhs, rhs)

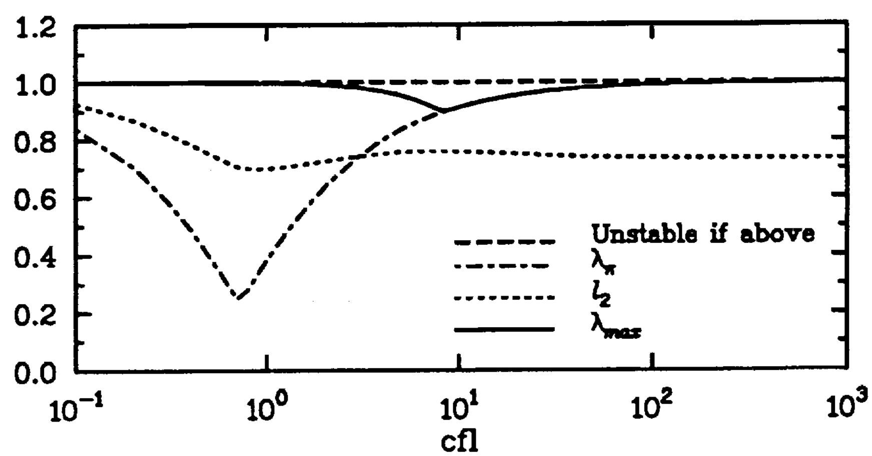

(b) Exact Jacobians (lhs, rhs)

Figs. (3a)–(3b): Eigenvalues for Linear Stability Analysis of 1–D Euler Equations (First–order lhs; second–order rhs)

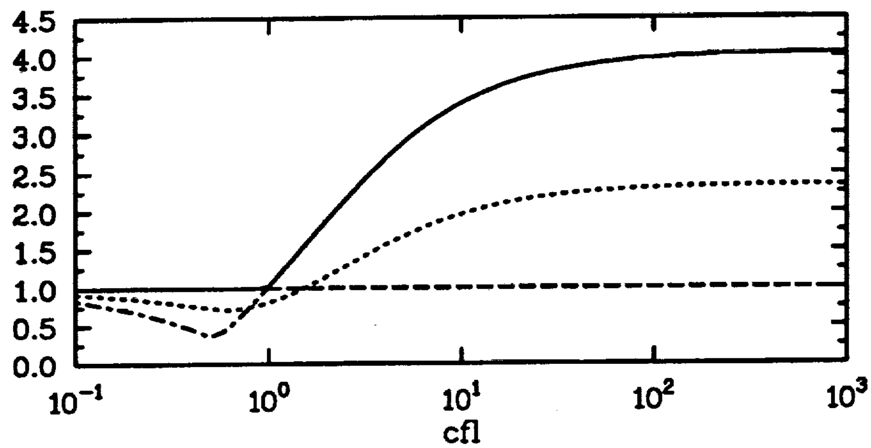

(c) Approx. Jacobians lhs; Exact Jacobians rhs

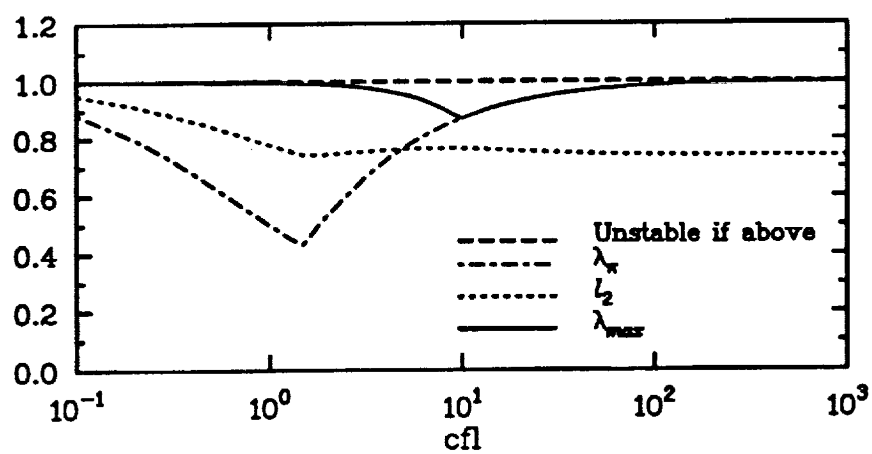

(d) Exact Jacobians lhs; Approx. Jacobians rhs

Figs. (3c)–(3d): Eigenvalues for Linear Stability Analysis of 1–D Euler Equations
(First–order lhs; second–order rhs)

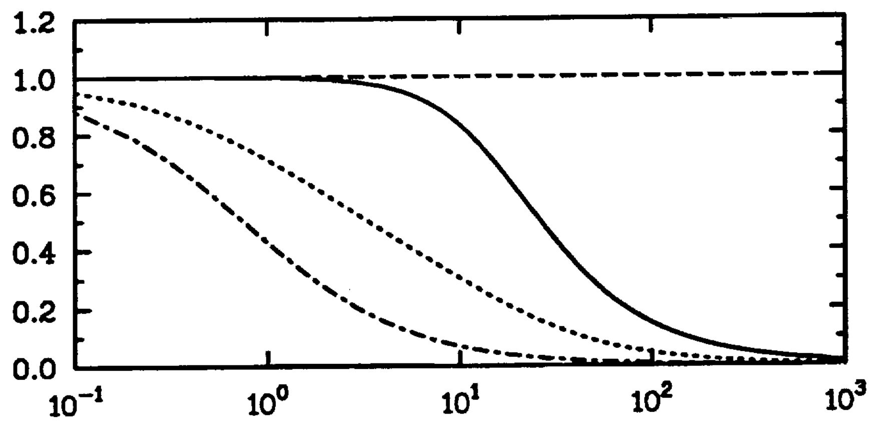

(a) Approx. Jacobians (lhs, rhs)

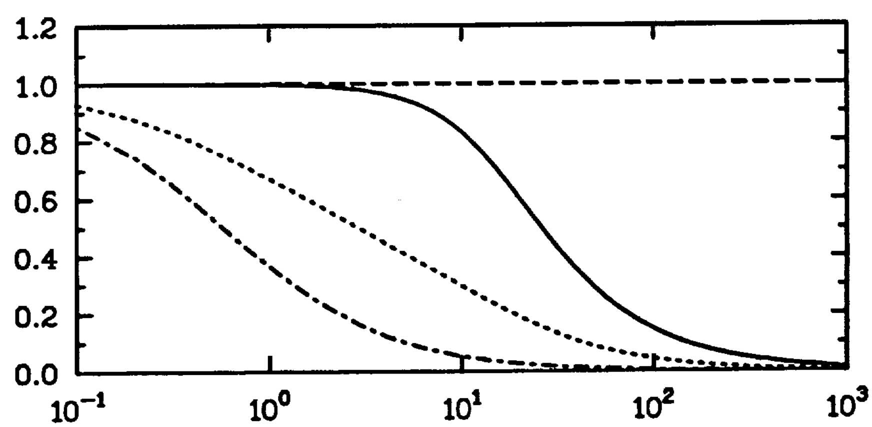

(b) Exact Jacobians (lhs, rhs)

Figs. (4a)–(4b): Eigenvalues for Linear Stability Analysis of 1–D Euler Equations (second–order both sides)

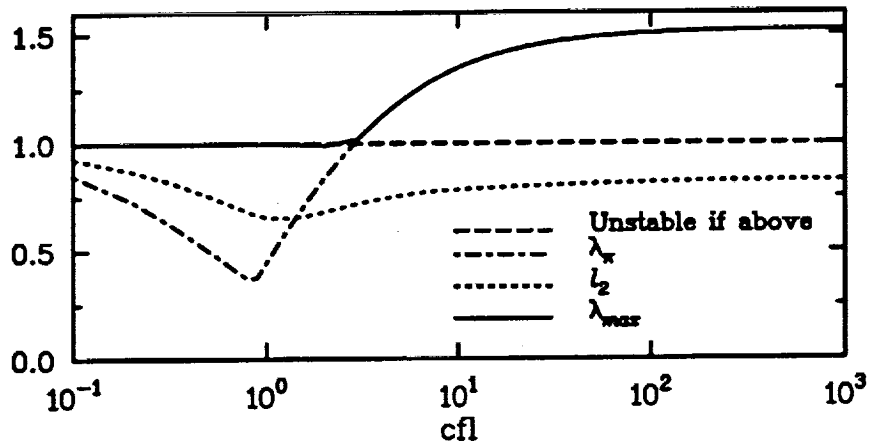

(c) Approx. Jacobians lhs; Exact Jacobians rhs

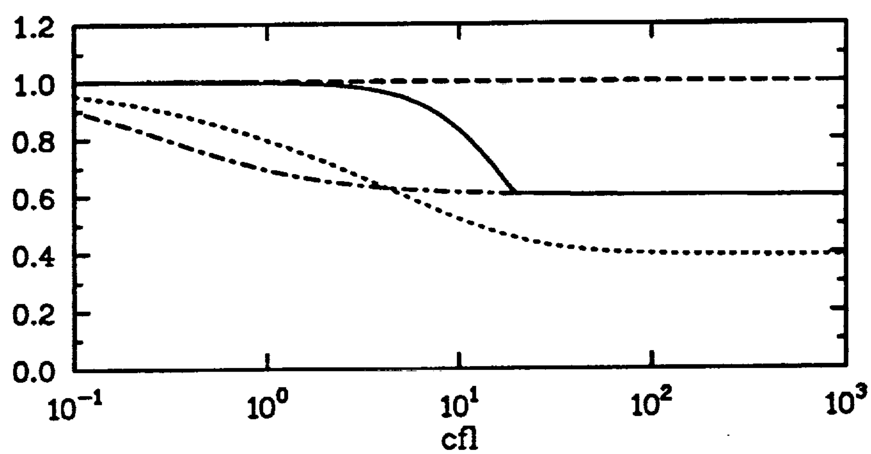

(d) Exact Jacobians lhs; Approx. Jacobians rhs

Figs. (4c)–(4d): Eigenvalues for Linear Stability Analysis of 1–D Euler Equations (second–order both sides)

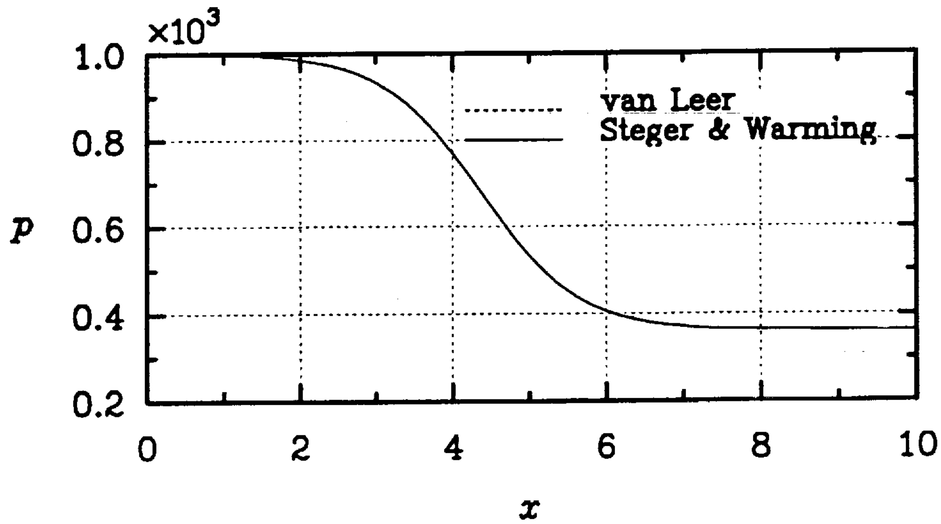

(a) Supersonic case

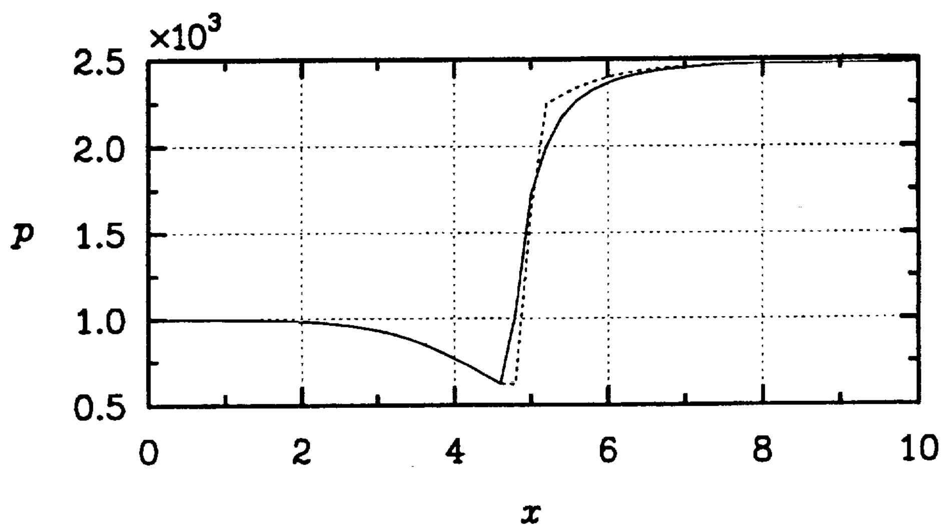

(b) Transonic case

Figs. (5a)–(5b): Steady solution of Quasi–1D Euler Equations (Pressure variation)

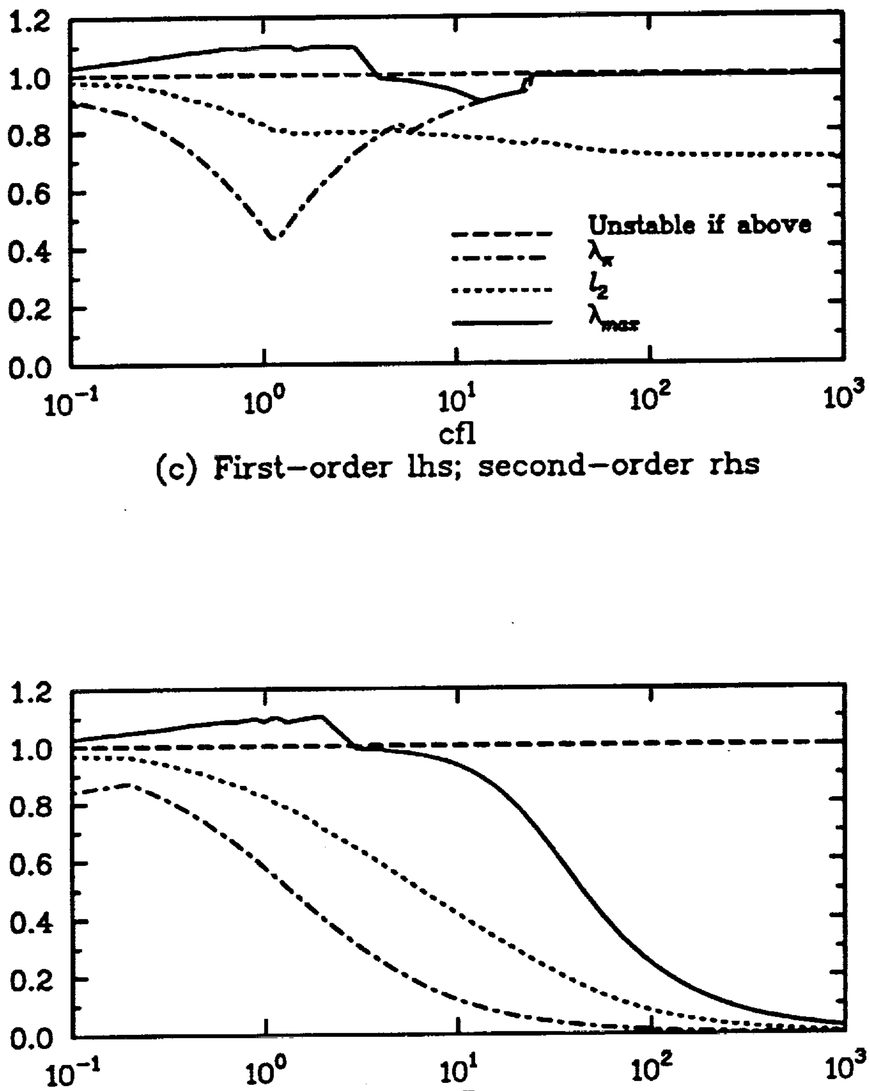

(c) First–order lhs; second–order rhs

(d) Second–order both sides

Figs. (5c)–(5d): Eigenvalues for Linear Stability Analysis of 1–D Euler Equations (Local Mode Analysis, Supersonic case)

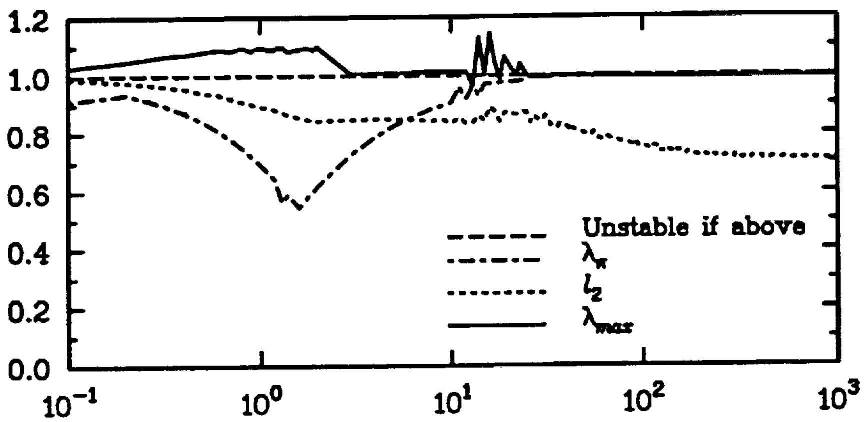

(e) First–order lhs; second–order rhs

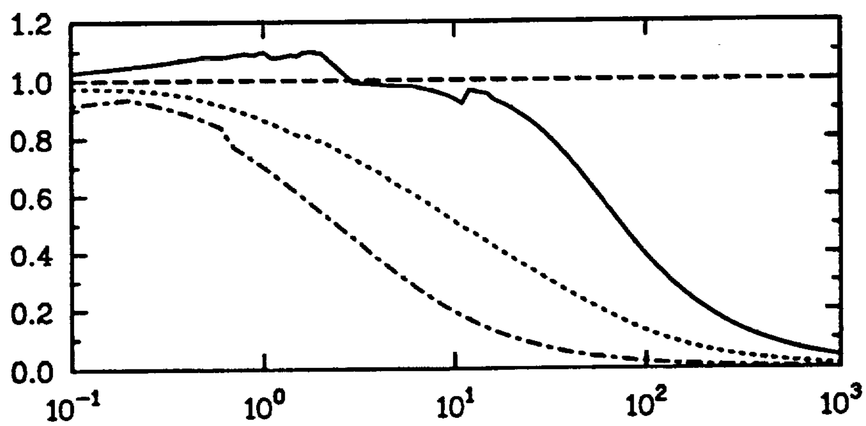

(f) Second–order both sides

Figs. (5e)–(5f): Eigenvalues for Linear Stability Analysis of 1–D Euler Equations (Local Mode Analysis, Transonic case)

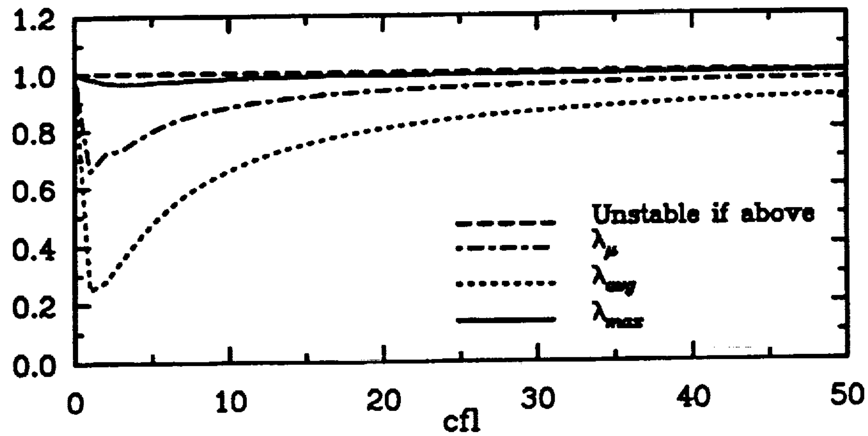

(a) $\kappa_2=0,\ \kappa_4=0.4$

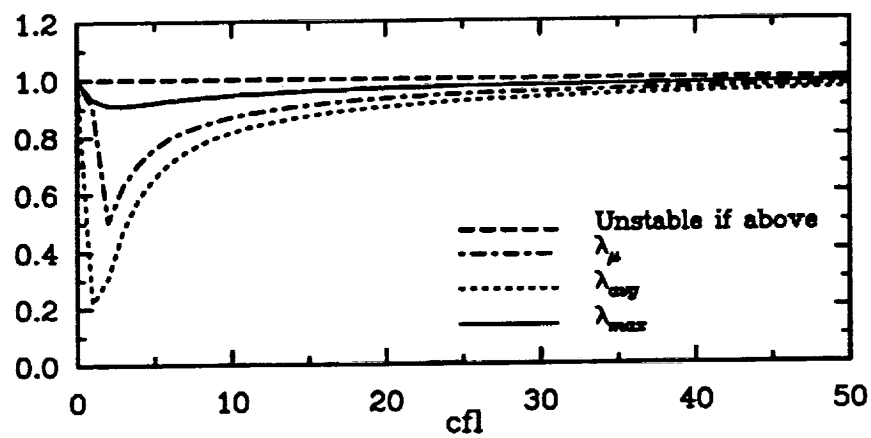

(b) $\kappa_2=2,\ \kappa_4=3$

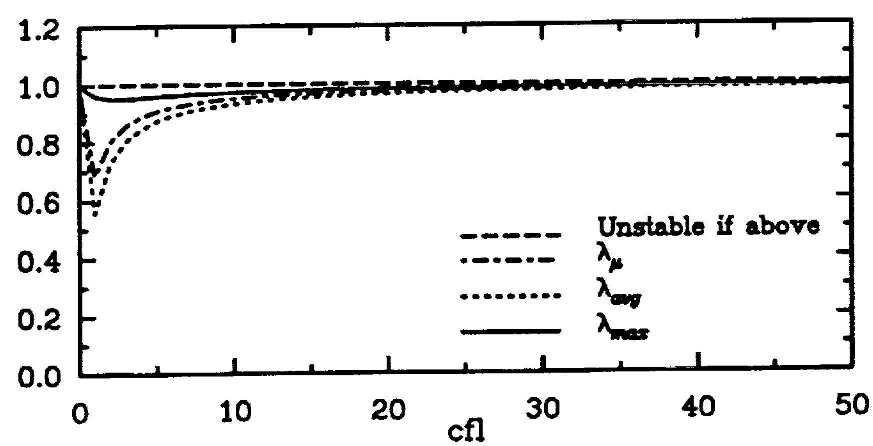

(c) $\kappa_2=3,\ \kappa_4=2$

Figs. (6a)–(6c): Eigenvalues for Linear Stability Analysis of 3–D Euler Equations (LU Factorization)

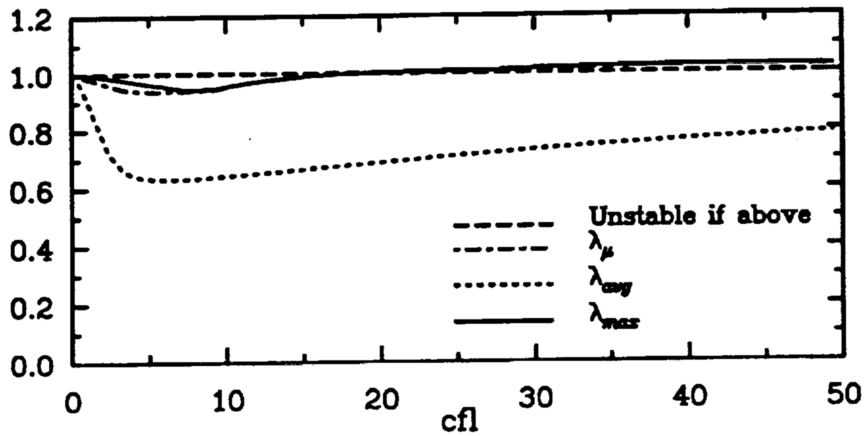

(a) ϵ_e=0, ϵ_i=0

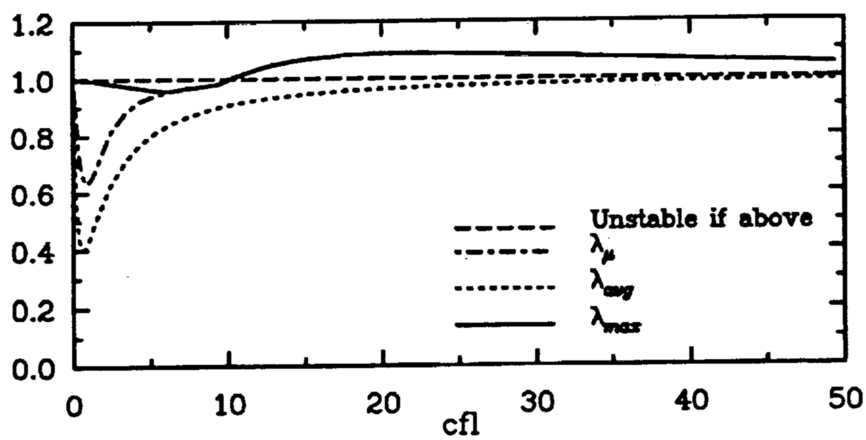

(b) ϵ_e=0.5, ϵ_i=1

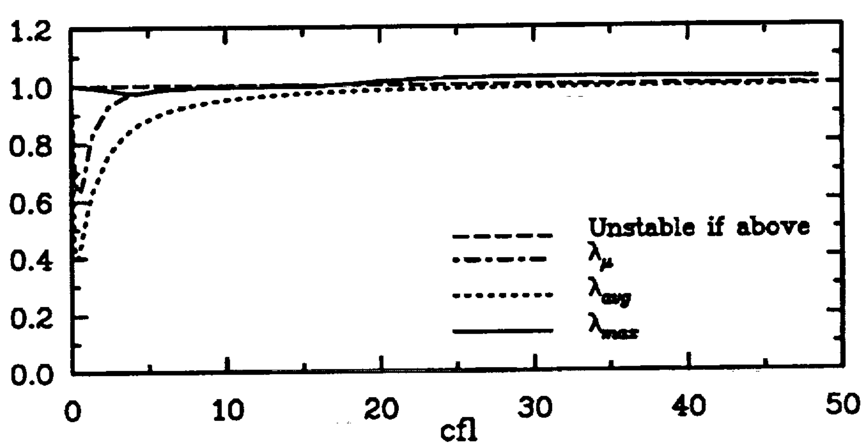

(c) ϵ_e=1, ϵ_i=2

Figs. (7a)–(7c): Eigenvalues for Linear Stability Analysis of 3–D Navier–Stokes Equations Beam and Warming's ADI Factorization: Re=1e2

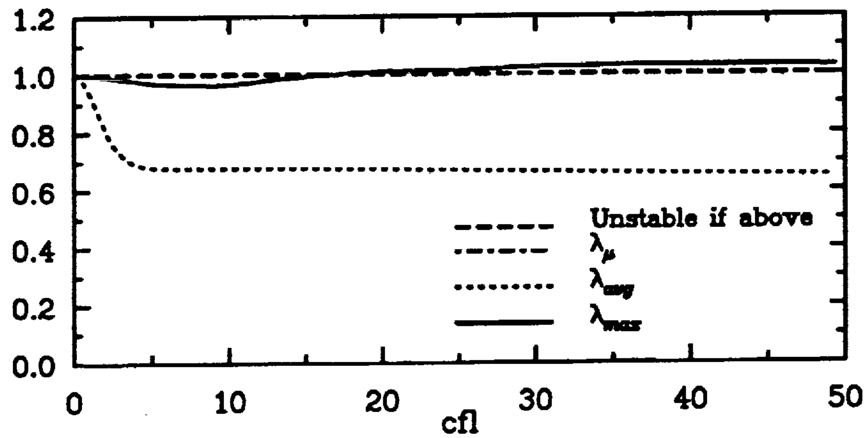

(a) ϵ_e=0, ϵ_i=0

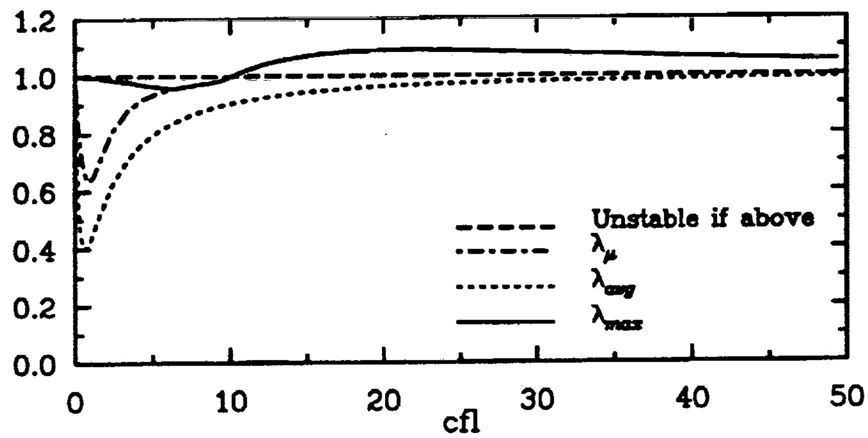

(b) ϵ_e=0.5, ϵ_i=1

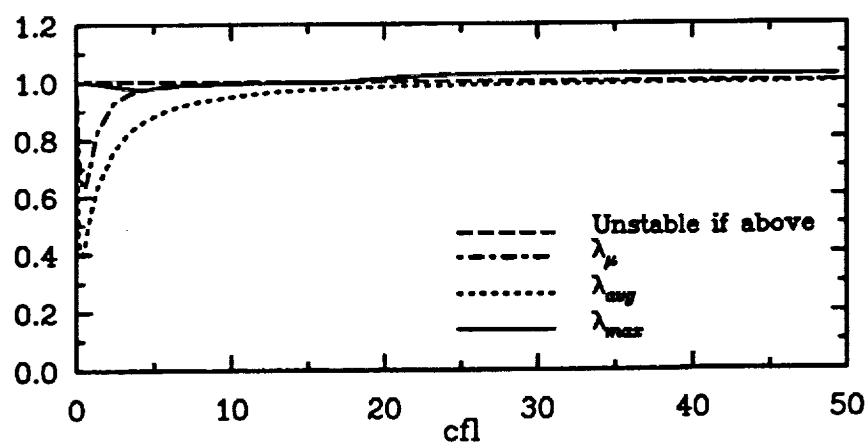

(c) ϵ_e=1, ϵ_i=2

Figs. (8a)–(8c): Eigenvalues for Linear Stability Analysis of 3–D Navier–Stokes Equations Beam and Warming's ADI Factorization: Re=1e6

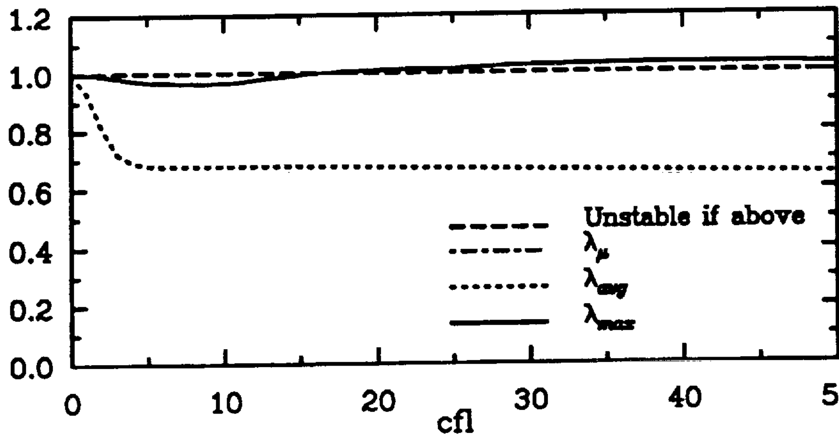

(a) $\epsilon_e=0$, $\epsilon_i=0$

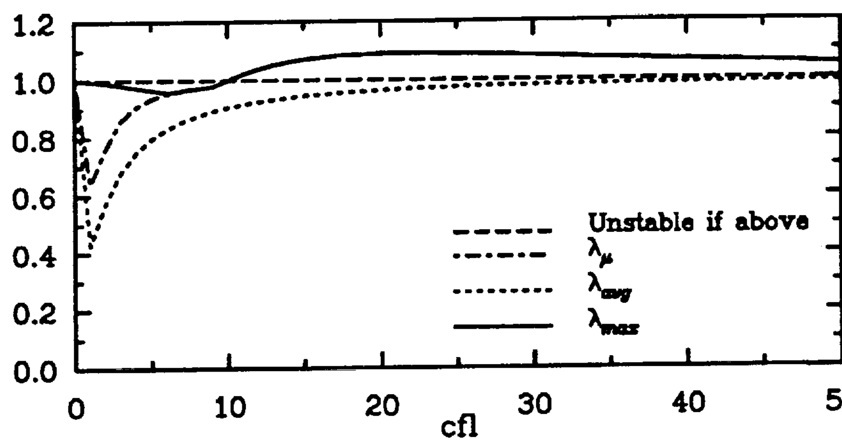

(b) $\epsilon_e=0.5$, $\epsilon_i=1$

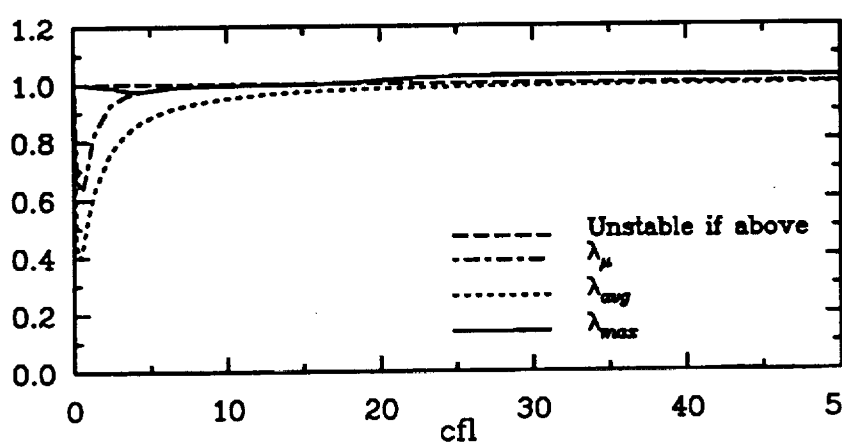

(c) $\epsilon_e=1$, $\epsilon_i=2$

Figs. (9a)–(9c): Eigenvalues for Linear Stability Analysis of 3–D Euler Equations Beam and Warming's ADI Factorization

REPORT DOCUMENTATION PAGE

Form Approved
OMB No. 0704-0188

1. AGENCY USE ONLY *(Leave blank)*

2. REPORT DATE
October 1993

3. REPORT TYPE AND DATES COVERED
Technical Memorandum

4. TITLE AND SUBTITLE
On the Stability Analysis of Approximate Factorization Methods for 3D Euler and Navier-Stokes Equations

5. FUNDING NUMBERS
WU–505–90–5K

6. AUTHOR(S)
A.O. Demuren and S.O. Ibraheem

7. PERFORMING ORGANIZATION NAME(S) AND ADDRESS(ES)
National Aeronautics and Space Administration
Lewis Research Center
Cleveland, Ohio 44135–3191

8. PERFORMING ORGANIZATION REPORT NUMBER
E–8054

9. SPONSORING/MONITORING AGENCY NAME(S) AND ADDRESS(ES)
National Aeronautics and Space Administration
Washington, D.C. 20546–0001

10. SPONSORING/MONITORING AGENCY REPORT NUMBER
NASA TM–106314
ICOMP–93–29

11. SUPPLEMENTARY NOTES
A.O. Demuren, Institute for Computational Mechanics in Propulsion, Lewis Research Center, and Old Dominion University, Department of Mechanical Engineering and Mechanics, Norfolk, Virginia 23529 and S.O. Ibraheem, Old Dominion University, Department of Mechanical Engineering and Mechanics, Norfolk, Virginia 23529, (work funded under NASA Cooperative Agreement NCC3–233). ICOMP Program Director, Louis A. Povinelli, (216) 433–5818.

12a. DISTRIBUTION/AVAILABILITY STATEMENT
Unclassified - Unlimited
Subject Category 64

12b. DISTRIBUTION CODE

13. ABSTRACT ***(Maximum 200 words)***

The convergence characteristics of various approximate factorizations for the 3D Euler and Navier-Stokes equations are examined using the von-Neumann stability analysis method. Three upwind-difference based factorizations and several central-difference based factorizations are considered for the Euler equations. In the upwind factorizations both the flux-vector splitting methods of Steger and Warming and van Leer are considered. Analysis of the Navier-Stokes equations is performed only on the Beam and Warming central-difference scheme. The range of CFL numbers over which each factorization is stable is presented for one-, two- and three-dimensional flow. Also presented for each factorization is the CFL number at which the maximum eigenvalue is minimized, for all Fourier components, as well as for the high frequency range only. The latter is useful for predicting the effectiveness of multigrid procedures with these schemes as smoothers. Further, local mode analysis is performed to test the suitability of using a uniform flow field in the stability analysis. Some inconsistencies in the results from previous analyses are resolved.

14. SUBJECT TERMS
Stability analysis; Approximate factorization; Euler and Navier-Stokes equations

15. NUMBER OF PAGES
38

16. PRICE CODE
A03

17. SECURITY CLASSIFICATION OF REPORT	18. SECURITY CLASSIFICATION OF THIS PAGE	19. SECURITY CLASSIFICATION OF ABSTRACT	20. LIMITATION OF ABSTRACT
Unclassified	Unclassified	Unclassified	